Chaotic versus stochastic behavior in active-dissipative nonlinear systems

Chaotic versus stochastic behaviour in active-dissipative nonlinear systems

Hiroshi Gotoda[1], Marc Pradas[2], and Serafim Kalliadasis[3]
[1] *Department of Mechanical Engineering, Tokyo University of Science, 6-3-1 Niijuku, Katsushika-ku, Tokyo, 125-8585, Japan*
[2] *School of Mathematics and Statistics, The Open University, Milton Keynes MK7 6AA, UK*
[3] *Department of Chemical Engineering, Imperial College London, London SW7 2AZ, UK*

We study the dynamical state of the one-dimensional noisy generalized Kuramoto-Sivashinsky (gKS) equation by making use of time-series techniques based on symbolic dynamics and complex networks. We focus on analyzing temporal signals of global measure in the spatiotemporal patterns as the dispersion parameter of the gKS equation and the strength of the noise are varied, observing that a rich variety of different regimes, from high-dimensional chaos to pure stochastic behaviour, emerge. Permutation entropy, permutation spectrum and network entropy allow us to fully classify the dynamical state exposed to additive noise.

I. INTRODUCTION

External or internal random fluctuations are well-known to have significant impact on the formation of complex spatiotemporal patterns in a wide spectrum of biological, engineering and physical environments, with several examples in the context of fluid dynamics, e.g. Rayleigh-Bénard convection [1, 2], contact line dynamics [3, 4], or waves on free-surface thin-film flows [5, 6]. Many of these systems can be modeled by noisy spatially extended systems (SES) described through stochastic partial differential equations (SPDEs) in large or unbounded domains. SES are typically characterized by the presence of a wide range of length and time scales which non-trivially interact with each other and which often leads to complex spatiotemporal behavior, such as for example noise-induced phenomena including spatial patterns and phase transitions [7–11].

A well-known prototype is the Kuramoto-Sivashinsky (KS) equation, a paradigmatic example of SES exhibiting sptatiotemporal chaos, which has been shown to be applicable in a wide spectrum of physical settings, including hydrodynamic (e.g. thin-film) instabilities [12, 13] and optics such as bright spots formed by self-forcing of the beam profile [14]. For thin film flows in particular, such as falling films, the KS equation is obtained via a weakly nonlinear expansion of the 1D Navier-Stokes equations subject to wall and free-surface boundary conditions and assuming strong surface tension effects–long waves [15]. With the addition of noise, the stochastic version of this equation, the noisy KS equation, has been used as a prototype for a wide spectrum of nonlinear systems, e.g. wave evolution of thin films through sputtering processes, and ion beam-erosion induced nanostructures on solid surfaces [16–23]. A key point in these studies was the understanding of emergence of underlying scaling growth laws as a consequence of kinetic roughening processes. Moreover, it has recently been shown that the noisy KS solution close to the instability onset may undergo several non-trivial critical transitions between different dynamical states corresponding to dynamic phase transitions, including intermittency, as the noise intensity is increased [24, 25]. A rigorous justification of the presence of noise and stochastic effects as a result of stochastic mode reduction (using elements from evolutionary renormalisation group theory together with the principle of maximum information entropy) has been recently given in Refs. [26, 27].

Likewise, a more general version of the deterministic KS equation which includes dispersive effects, and is often referred to as the generalized KS (gKS) equation, has been used in a wide variety of contexts, such as reactive and falling films [28–30], films falling down a uniformly heated wall [31] and a vertical fiber [32], two-phase flows with surfactants [33], plasma waves with dispersion [34], and step dynamics [35–37], amongst others. An extended version that includes the Hilbert transform operator has also been derived for modeling a conducting liquid film dynamics exposed to an external electric field [38], while different methodologies to control the solution of the gKS equation have been proposed recently [39, 40].

The key feature of the gKS equation is that for sufficiently small dispersion effects its dynamical behaviour resembles the high-dimensional spatiotemporal chaos of the deterministic KS solution, while sufficient large dispersion effects tends to regularise and arrest the usual KS spatiotemporal chaos in favor of spatially periodic travelling waves, which are very common in falling liquid films [41]. This effect has been intensively studied via coherent-structure theories [42–49]. In addition, we have ourselves recently investigated the transition process from high-dimensional to low-dimensional chaos in the gKS equation owing to the appearance of dispersion effects [52]. However, there are no detailed studies on how the presence of additive noise may affect the overall behaviour of the gKS solution, particularly understanding the interplay between dispersion and additive noise effects. This is relevant for many different applications such as, e.g., in the context of thin-film hydrodynamics, where noise may enter the system via perturbations on the solid substrate boundary [25], or through thermal fluctuations for which one needs to consider the

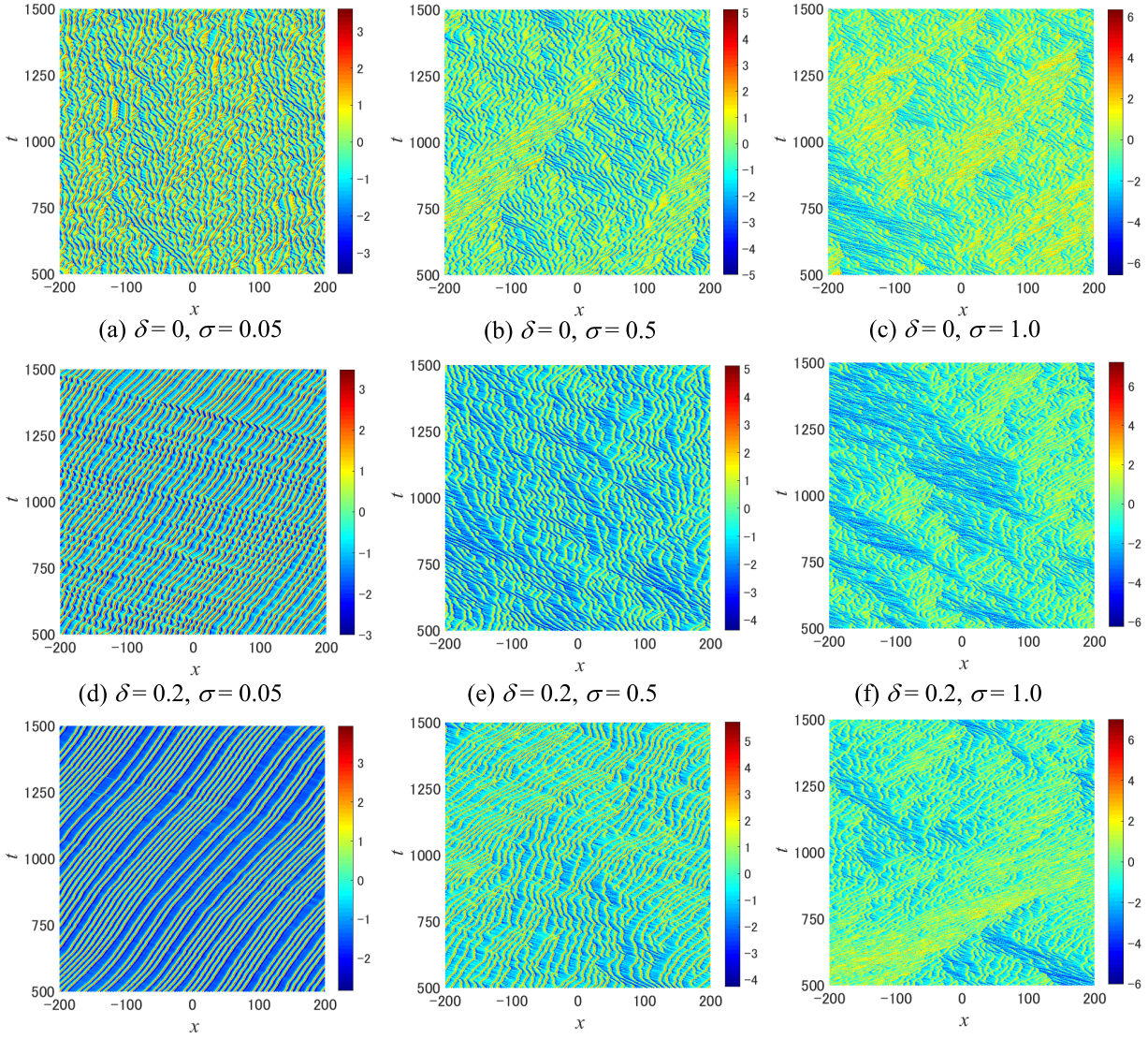

FIG. 1: Spatiotemporal patterns of the noisy gKS solution for different values of σ and δ.

stochastic Navier-Stokes equations to obtain a simplified thin-film partial differential equation that includes stochastic effects [53, 54].

Our overarching objective here is precisely the understanding of this interplay but also to reveal how additive noise alters the dynamical states of the noisy gKS equation. To this end, we adopt two time-series analyses in terms of symbolic dynamics, namely the permutation entropy and the permutation spectrum proposed by Kulp and Zunino [56] as a means to distinguish between chaotic and stochastic dynamics. In relation to the Shannon entropy, another useful measure in terms of complex networks, referred to as the network entropy, has been proposed by Luque *et al.* [57]. This considers the probability distribution of the degree in the horizontal visibility graph, and can capture the significant transition to chaos via period-doubling bifurcation process. We also attempt to distinguish between chaotic and stochastic dynamics from the viewpoint of complex network.

Using these methodologies, we show that the noisy gKS solution exhibits a very rich dynamics as the two relevant parameters, namely the parameter controlling dispersive effects and the noise intensity, are varied, observing that the dynamics can be classified into three distinct regimes: deterministic chaotic regime, co-existence regime of chaos and noise, and purely stochastic regime. We also show that these methodologies based on symbolic dynamics and complex networks are more powerful to distinguish between chaos and stochasticity than other more standard techniques such as power spectral density and nonlinear forecasting methods.

II. SPATIOTEMPORAL DYNAMICS OF THE NOISY GKS EQUATION

We consider the noisy gKS equation:

$$\frac{\partial u}{\partial t} + u\frac{\partial u}{\partial x} + \frac{\partial^2 u}{\partial x^2} + \delta\frac{\partial^3 u}{\partial x^3} + \nu\frac{\partial^4 u}{\partial x^4} + \sigma\zeta(x,t) = 0, \tag{1}$$

in a periodic domain $[-L, L]$, i.e. of size $2L$, where $\zeta(x,t)$ is a Gaussian stochastic process with properties $\langle\zeta(x)\rangle = 0$ and $\langle\zeta(x,t)\zeta(x',t')\rangle = 2\delta(x-x')\delta(t-t')$; and σ represents the strength of the noise. The parameters ν and δ characterize viscosity damping and relative importance of dispersion, respectively. It is noteworthy that a detailed derivation of the noisy KS equation in the context of thin-film hydrodynamics, i.e. externally forced falling liquid films, is given in Ref. [25]. This can be appropriately modified to obtain the noisy gKS equation; after all, the KS equation is the relevant prototype for falling films close to criticality, while really close to criticality the KS equation is replaced by the gKS one. In this context the parameter δ is related to the Reynolds number, Re, and Weber number, We, as $\delta = \sqrt{15/2(Re - Re_c)We}$, where Re_c represents the critical Reynolds number [41]. The control of the noisy gKS equation was considered in the recent study in Ref. [63].

Some previous studies on the KS equation [58, 59] have reported that for sufficiently large L, many Fourier modes are active and the transition to spatiotemporal chaos becomes independent of L. On this basis, an extended computational domain with $L = 500$ is discretized into $N_L = 5000$ points. Equation (1) is then numerically solved by adopting a pseudo-spectral method for the spatial derivatives that uses the Fast Fourier Transform (FFT) to transform the $u(x,t)$ solution to Fourier space with wavenumber $k \in [-\pi/\Delta x, \pi/\Delta x]$ so that aliasing is avoided [60] and where $\Delta x = L/N_L$. The nonlinear term is evaluated in real space and transformed back to Fourier space by using the inverse FFT. The solution is then propagated in time by making use of a modified fourth-order exponential time-differencing-time-stepping Runge-Kutta (ETDRK4) scheme [61, 62] with a time step $\Delta t = 0.1$, and a sampling time interval of $dt = 1$. The additive noise is numerically introduced by considering its Fourier representation: $\zeta(x,t) = \sum_k W_k(t)\exp(ikx)$, where $W_k(t)$ is a Gaussian white noise with $W_{-k} = W_k^*$, with the star denoting its complex conjugate. We impose a random initial condition as $u(x,0) = \xi(x)$ with $\langle\xi(x)\rangle = 0$ and $\langle\xi(x)\xi(x')\rangle = 2\delta(x-x')$. We choose $\nu = 1$ and vary the dispersion parameter δ from 0 to 2 so that the underlying deterministic dynamics undergoes a transition from high-dimensional chaos to periodic solutions [52]. Note that we ensure that the probability density function of the random initial conditions converges to a normal distribution of mean zero and variance one so that starting the computations with different random initial conditions has little influence on the gKS solutions.

Figure 1 depicts the spatiotemporal patterns of the noisy gKS equation for different values of δ and σ. For $\delta = 0$ (which corresponds to the KS solution), we observe that for small values of the additive noise strength deterministic high-dimensional chaos is observed but this tends to disappear as σ is increased, observing a noisy pattern, as expected. For $\delta = 0.2$ and $\delta = 0.4$, the emergence of localized coherent structures starts to be important which in turn gives rise to a regime of low-dimensional chaos [52], also known as "interfacial turbulence in the Manneville sense" [41, 64]. We can see that this regime is still retained for sufficiently small values of the noise strength but it appears to be more sensitive to variations in σ than the high-dimensional chaos regime observed at $\delta = 0$.

Our main goal is to quantify the dynamics of the noisy gKS solution by understanding how the different regimes of chaos and stochasticity appear and disappear in the parameter space defined by (σ, δ). To this end we shall make use of time-series analyses to study the time fluctuations of the global measure corresponding to the second moment of the noisy gKS solution which is defined as follows:

$$u_G(t) \equiv \frac{1}{2L}\int_{-L}^{L}[u(x,t) - \overline{u}(t)]^2 \mathrm{d}x, \tag{2}$$

where the overbar denotes spatial average.Figure 2 shows typical evolutions of the signal $u_G(t)$ for $\delta = 0$ and different values of σ. It is important to remark that one of the reasons of choosing such a global quantity is because global quantities are often easier to obtain experimentally than e.g. local measures. We also note that as it has recently been shown in Ref. [52], global and local quantities give qualitative similar descriptions of the deterministic gKS system.

III. TIME-SERIES ANALYSES METHODOLOGIES

We briefly review here some of the methodologies adopted in this study to quantify the dynamics of the temporal global measure $u_G(t)$ and which have been recently proposed in the literature.

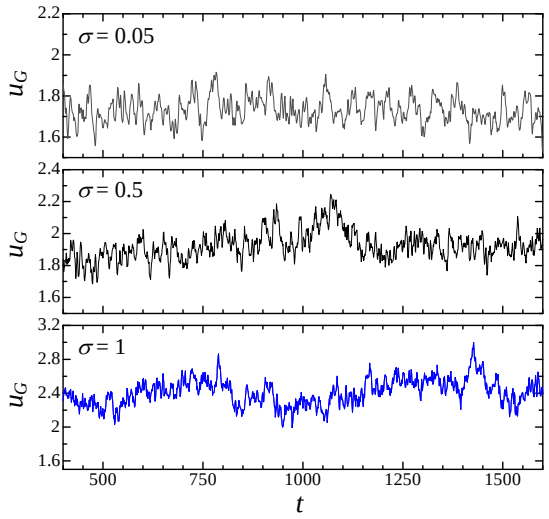

FIG. 2: Time variation of the signal u_G for $\delta = 0$ and different values of σ.

A. Permutation entropy and permutation spectrum

Permutation entropy [55] is used to estimate the degree of randomness from a sequence of ranks in the values of a time series, and it has been shown to capture the complexity of the dynamics observed in a broad range of systems from physical sciences to engineering [65]. A modified version of it has also been recently proposed to quantify the complexity of heartbeat dynamics [66]. In this study, we use the permutation entropy to capture the changes in the dynamical state of the noisy gKS solution. For the estimation of the permutation entropy, we first set the order of the permutation, D_e, which is defined as the number of points in time series consisting of $\mathbf{u_G}(t_i) = (u_G(t_i), u_G(t_i+1), ..., u_G(t_i+D_e-1))$, where $i = 0, 1, \ldots, n$ with n being the number of values in the data set. We index all possible permutation patterns ($D_e!$ permutations) which we denote as π. We then calculate the probability, $p(\pi)$, of the existing patterns for all $\mathbf{u_G}(t_i)$. We note that each permutation represents a coarse-grained pattern in the temporal evolution of $u_G(t_i)$. Following the definition of Shannon entropy, the permutation entropy h_p is obtained as:

$$h_p = \frac{-\sum_{\pi} p_e(\pi)\log_2 p_e(\pi)}{\log_2 D_e!}. \tag{3}$$

We note that we include the normalization constant ($\log_2 D_e!$) so that the permutation entropy varies between $0 \leq h_p \leq 1$, where $h_p = 0$ corresponds to a monotonically increasing or decreasing process, while $h_p = 1$ corresponds to a completely random process.

On the other hand, we also consider the permutation spectrum which was proposed by Kulp and Zunino [56] and enables us to test for the existence of determinism underlying complex dynamics. In this method, the realization frequency for each sequence occurring in disjointed windows is calculated by iterating over the time series. The permutation spectrum consists of the frequency distribution of permutation patterns for each disjointed window and their standard deviation between the windows. The appearance of zero standard deviation with some forbidden patterns (original patterns that are absent in the frequency distribution) [56] indicates the presence of chaotic dynamics, while the dynamic behavior of u_G exhibits stochasticity if observing a non zero standard deviation and no forbidden patterns.

It should be noted that Bandt and Pompe [55] considered the permutation entropy considering the frequency of the rank order patterns with embedding dimension $3 \leq D_e \leq 7$ for the consecutive points of time series (time delay of phase space $\tau = 1$). In contrast, Kulp and Zunino [56] considered $D_e = 4$ and 5. In a preliminary test (not shown), we found that the forbidden patterns in the permutation spectrum appear even in stochastic dynamics, such as e.g. Brownian motion, under $D_e \geq 7$. This suggests that the embedding dimension with $D_e \leq 6$ should be considered for the computation of the permutation entropy. On the basis of this preliminary test and the work by Kulp and Zunino [56], we consider $D_e = 5$ as a suitable embedding dimension. Note that an advantage of the permutation entropy is that it is not necessary to consider the construction of high-dimensional phase space that is required for computation of the largest Lyapunov exponent and correlation dimension.

B. Network entropy

Luque et al. [57] have shown that the network structure in the horizontal visibility graph captures the sensitivity to initial condition in nonlinear dynamics due to orbital instability. On this basis, we estimate the network entropy in the visibility graph. We connect two nodes in the graph if $u_G(t_i)$ and $u_G(t_j)$ in the time series satisfy the geometrical criterion

$$u_G(t_i), u_G(t_j) > u_G(t_n), \quad \forall n \in (i, j). \tag{4}$$

Following the definition of the Shannon entropy, the network entropy h_n is obtained using the degree distribution in the graph.

$$h_n = -\sum_k p(k) \ln p(k), \tag{5}$$

where k is the degree and $p(k)$ is the degree distribution of the visibility graph. It should be noted that the permutation entropy considers local randomness between nearby discrete data points of time series, while the horizontal visibly graph consists of the connections between the discrete data points in unlimited width of window, or in other words, the network entropy incorporating the degree distribution represents the global randomness of time series. Hence, an important advantage of using the horizontal visibility graph is that it is not necessary to consider the window size of time series, i.e. it is not necessary to consider the embedding dimension corresponding to pattern-length. Recently, the permutation entropy and network entropy have been adopted for hydrodynamic transition to wave turbulence [67], which shows that the use of these entropies becomes important for classification of different dynamical behaviors in noisy deterministic data.

C. Nonlinear forecasting

Here we adopt our nonlinear forecasting methodology introduced in Ref. [52] to extract the predictability properties of the noisy gKS solution. Our methodology has also been applied successfully in a wide spectrum of different applications, from combustion instability in a thermoacoustic system [68] and radiative heat-loss-induced flame front instability [69]. In our methodology, we first divide a given temporal signal of $u_G(t)$ for $t \in [0, T_f]$ into two intervals, namely $t \in [0, t_L]$ and $t \in (t_L, T_f]$, corresponding to a library and test set, respectively. Note that T_f is the final time of the given temporal signal of $u_G(t)$. The library data is used to predict the temporal signal of $u_G(t)$. The test set is used to compare with the predicted temporal signal of $u_G(t)$ for $t > t_L$. We adopt Taken's embedding theorem [70] to construct the vectors in a D-dimensional phase space consisting of $\mathbf{u_G}(t_i) = (u_G(t_i), u_G(t_i - \tau), ..., u_G(t_i - (D-1)\tau))$ where τ is a lag time which is estimated by the mutual information, in a similar way as done in Refs. [52, 68, 71]. In addition, we set $D = 5$ to nonlinear forecasting the signal $u_G(t)$. We define $\mathbf{u_G}_f \equiv \mathbf{u_G}(t_f)$ as the last point of a trajectory in the phase space constructed from the reference data. Neighboring vectors, denoted by $\mathbf{u_G}_k$, to the vector $\mathbf{u_G}_f$ are searched from all data points in the phase space. We denote the predicted value corresponding to $\mathbf{u_G}_k$ after T as $u_G(t_k + T)$, and then predict $\check{u}_G(t_f + T)$ by Eq. (6):

$$\check{u}_G(t_f + T) = \frac{\sum_{k=1}^{K} u_G(t_k + T) \mathrm{e}^{-d_k}}{\sum_{k=1}^{K} \mathrm{e}^{-d_k}}, \tag{6}$$

which consists of a nonlinearly weighted sum of the library data $u_G(t_k + T)$, where d_k is the Euclidian distance between $\mathbf{u_G}_f$ and $\mathbf{u_G}_k$. We then compare the predicted $\check{u}_G(t_f + T)$ and the test set $u_G(t_f + T)$ by estimating the correlation factor defined as:

$$C = \frac{\mathbb{E}[u_G(t)\check{u}_G(t)]}{\sigma_{u_G}\sigma_{\check{u_G}}}, \tag{7}$$

where $\mathbb{E}[u(t)\check{u_G}(t)]$ denotes the covariance between both signals, and σ_{u_G} and $\sigma_{\check{u_G}}$ are the standard deviation of u_G and $\check{u_G}$, respectively. The relation between correlation coefficient C and predicted time t_P allows us to extract the short-term predictability and long-term unpredictability characteristics of the dynamics, as proposed in our recent study on the deterministic gKS equation [52].

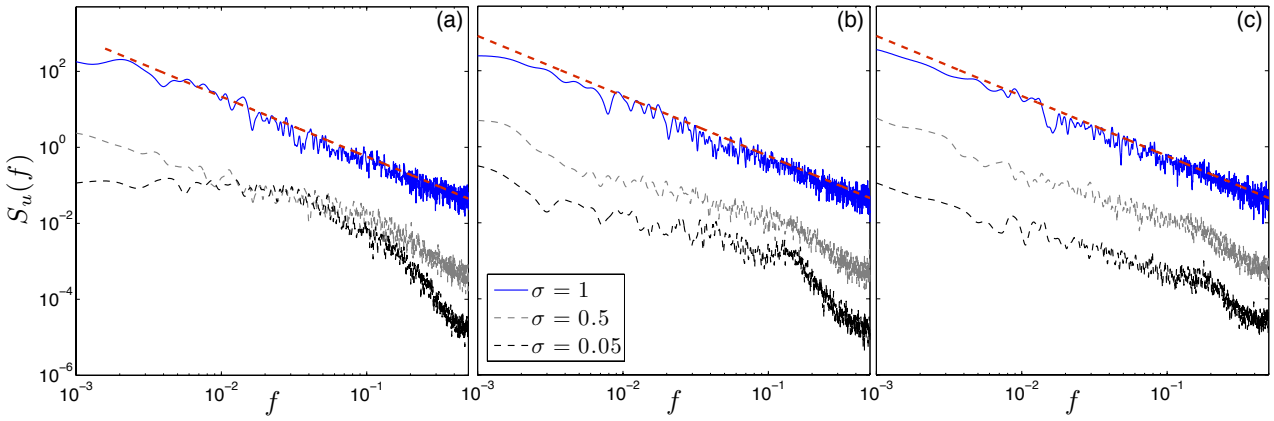

FIG. 3: Power spectrum density $S_u(f)$ for different values of σ and for $\delta = 0$ (a), $\delta = 0.2$ (b), and $\delta = 0.4$ (c). The red dashed line corresponds to a power law with exponent -1.56 ± 0.08.

IV. NUMERICAL RESULTS OF THE NOISY GKS EQUATION

We present here the analysis of the time series $u_G(t)$, computed from the gKS solution. Since we are comparing chaotic to stochastic regimes, all the methodologies which we use to analyse the noisy gKS solution will also be applied to a reference pure stochastic signal which we choose it to be a solution of a simple and well-known SPDE. In particular, we consider the Edward-Wilkinson (EW) equation [72], which was derived to physically understand stochastic particle sedimentation, and is the simplest linear stochastic equation for describing the growing interface roughness which is governed by the interplay between surface tension and noise:

$$\frac{\partial u}{\partial t} = \frac{\partial^2 u}{\partial x^2} + \sigma\zeta(x,t), \tag{8}$$

where $\zeta(x,t)$ is a Gaussian white noise with same properties as in Eq. (1). We compute the corresponding global signal u_G for the EW equation and we analyse it by making use of time series analysis. This will be used for comparison with the noisy gKS solutions.

A. Power spectrum

We start by making use of some standard tools for time signals analysis. In particular, we analyze the power spectral density (PSD) of u_G which is defined as $S_u(f) = |\langle \hat{u}_G(f)|^2\rangle$. Here, $\hat{u}_G(f)$ represents the Fourier transform of $u_G(t)$ in the frequency domain, and the symbols $\langle \dots \rangle$ denote average over different time intervals - we note we are assuming statistically stationary solutions. Figure 3 shows the PSD for different values of σ and δ covering the high-dimensional chaos regime (which is obtained for $\delta = 0$) to low-dimensional chaos ($\delta = 0.4$). We observe that the PSD changes from being exponentially decaying at small values of the noise intensity, an important feature of chaotic signals, to exhibiting a power-law decay with exponent -1.56 ± 0.08 at sufficiently large values of the noise intensity, a feature typically connected with stochastic processes. In this sense, the noisy gKS equation includes a regime where both stochastic effects and low-dimensional chaos are competing at different scales (we note that coherent structures are constantly interacting with each other while noise is acting as a constant destabilising mechanism), which is typical of turbulent-like systems.

B. Permutation entropy, permutation spectrum and network entropy

Figure 4 depicts the permutation entropy h_p as function of δ and σ. Note that we use the value of h_p for the EW solution as a reference of a pure stochastic process, which gives a numerical value of $h_p \sim 0.9$ and remains constant regardless of σ (see solid line in Fig. 4(a)). We observe that h_p for $\delta = 0$ remains constant at around $h_p \leq 0.7$ with increasing the noise intensity up to a critical value $\sigma \sim 0.07$, indicating that for these values the signal remains chaotic. As σ keeps increasing, the permutation entropy starts to gradually increase until it reaches a similar value as for the EW solution, indicating that at this point the signal is fully stochastic. A similar trend is observed for values

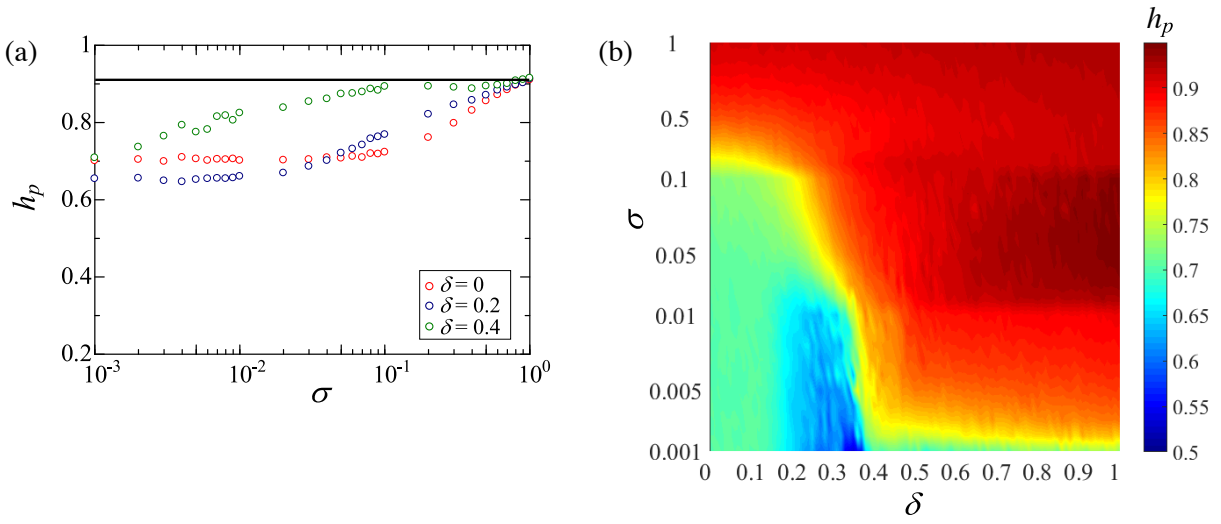

FIG. 4: (a) Permutation entropy h_p as function of σ for $\delta = 0$, 0.2, and 0.4. The solid line corresponds to the permutation entropy obtained from the EW equation. (b) Surface plot of h_p as function of δ and σ.

of δ up to 0.2 (see Fig. 4(a)), albeit the critical value decreases as δ is increased. For values of $\delta > 0.2$ we observe that the permutation entropy keeps increasing until it becomes nearly constant around the value of the EW equation, indicating that for relatively large values of δ the signal becomes purely stochastic independently of σ. Figure 4(b) shows a phase diagram of these different dynamical states where we can see a clear continuous transition between a chaotic state (which we can define it to be for $h_p < 0.7$) and a stochastic regime ($h_p > 0.8$).

Similar behaviours are detected by looking at the permutation spectrum and the network entropy. Figure 5 depicts the permutation spectrum (both frequency distribution of permutation pattern for each sequence in disjointed windows and their standard deviation) for the noisy gKS with $\delta = 0.2$ and EW solutions. For low noise intensities, say $\sigma = 0.05$, we observe two dominant peaks corresponding to a monotonically increasing (permutation pattern $\pi_1 = 12345$) and decreasing process ($\pi_{120} = 54321$), and some distinct peaks (e.g. $\pi_{25} = 21345$, $\pi_{49} = 31245$, $\pi_{72} = 35421$, $\pi_{96} = 45321$) with relatively high frequency. As remarked in [56], the appearance of this type of peaks and forbidden patterns in the standard deviation between windows shows the strong persistence of deterministic dynamics. When σ is increased to 0.5, the frequency of these dominant peaks significantly decreases, and other permutation patterns appear due to a loss of determinism. The forbidden patterns vanish at high noise intensity $\sigma = 1.0$, showing that the dynamical behavior is dominated by stochastic process. For the EW solution, some distinct peaks are formed in the frequency distribution, but their degree is nearly the same level as the noisy-gKS solution at $\delta = 0.2$ and $\sigma = 1.0$. The number of forbidden patterns is zero regardless of σ (as it should be for purely stochastic dynamics). Variations in the number of forbidden patterns N_f normalized by the maximum number of possible forbidden patterns ($= D_e!$) are shown in Fig. 6(a) as functions of δ and σ. On the other hand, we observe that the network entropy, as defined in Eq. (5), exhibits a similar pattern in terms of δ and σ to that of both the permutation entropy and the number of forbidden patterns (see Fig. 7).

These numerical results allow us to conclude that the noisy gKS equation exhibits a rich dynamics which can be classified into three regimes: deterministic chaotic regime, co-existence regime of chaos and noise, and stochastic regime. We note that with the statistical tools used above we can quantify the transition from the *mixed* chaotic/stochastic regime to the *full* stochastic regime as σ is increased by measuring the critical value of the noise strength, say σ_c, at which the noisy gKS equation resembles the EW equation. For example, Fig. 6(b) shows the critical noise strength, σ_c defined as the value at which the number of forbidden patterns is zero (note that a similar analysis could be done from the permutation or network entropies). We observe that as δ is varied, the numerical data can be fit to a function of the form:

$$\sigma_c = \begin{cases} \sigma_1 \, e^{-\delta/\delta_p} & \text{if } \delta < \delta_c, \\ \\ \sigma_2 & \text{if } \delta > \delta_c, \end{cases} \tag{9}$$

with $\sigma_1 \simeq 0.56$, $\sigma_2 \simeq 0.026$, $\delta_p \simeq 0.15$ and $\delta_c \simeq 0.5$. We hence conclude that for values of $\delta < \delta_c$, the behaviour of the noisy gKS solution strongly depends on the strength of the noise, and chaotic dynamics can be observed even for relatively large noise intensities (up to $\sigma \simeq 0.56$). Such dependence, however, is exponentially suppressed as the dispersion parameter goes beyond the typical value $\delta_p \simeq 0.15$. It is interesting to note that this value of δ is very close

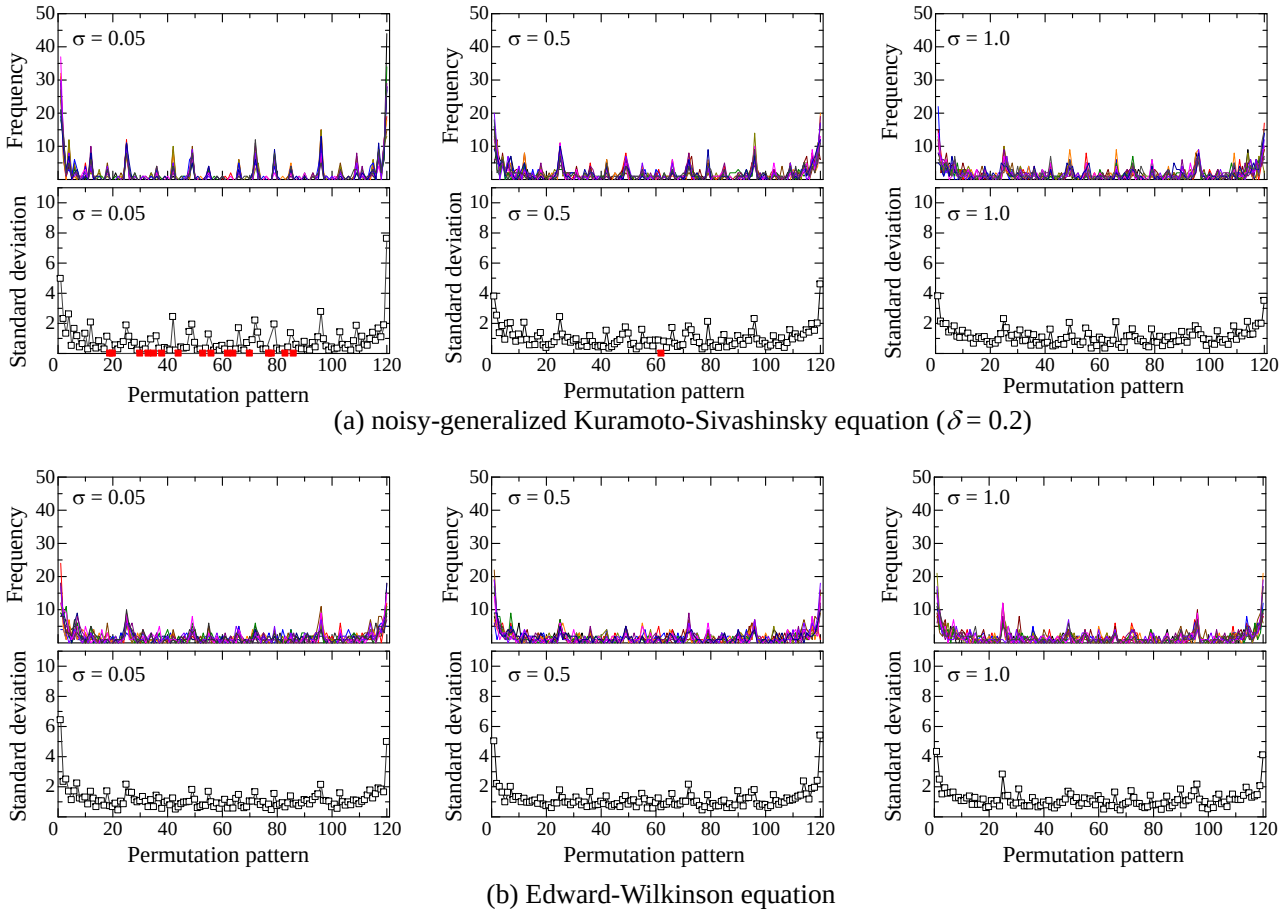

FIG. 5: Frequency distribution of permutation patterns of both the noisy gKS solution with $\delta = 0.2$ and EW solutions and their standard deviation at different σ. Forbidden patterns are shown as red dots.

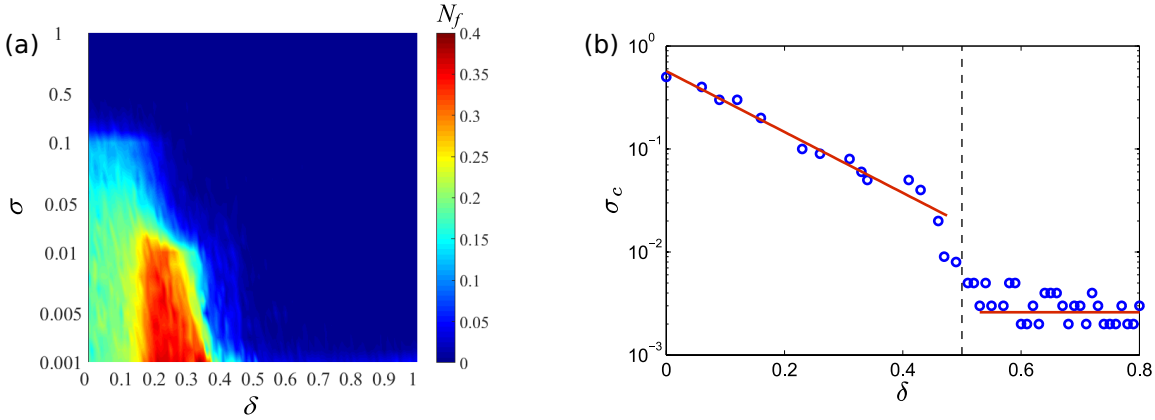

FIG. 6: (a) Number of forbidden patterns N_f of the noisy gKS solution as functions of δ and σ. (b) Critical value σ_c as function of δ above which the noisy gKS becomes fully stochastic. Solid lines correspond to a data fit to the function given by Eq. (9).

to the value reported in [49] where the stability of the deterministic gKS solution was studied and it was observed that above $\delta = 0.146$ pulse solutions become absolutely stable, demarcating the transition from high-dimensional to low-dimensional chaos. Therefore, the exponential decay of $\sigma_c(\delta)$ in the noisy gKS equation given by Eq. (9) can be understood in terms of the underlying transition occuring in the deterministic gKS as δ crosses δ_p. On the other hand, for $\delta > 0.5$ a minimum level of noise is sufficient to make the signal fully stochastic independently of δ.

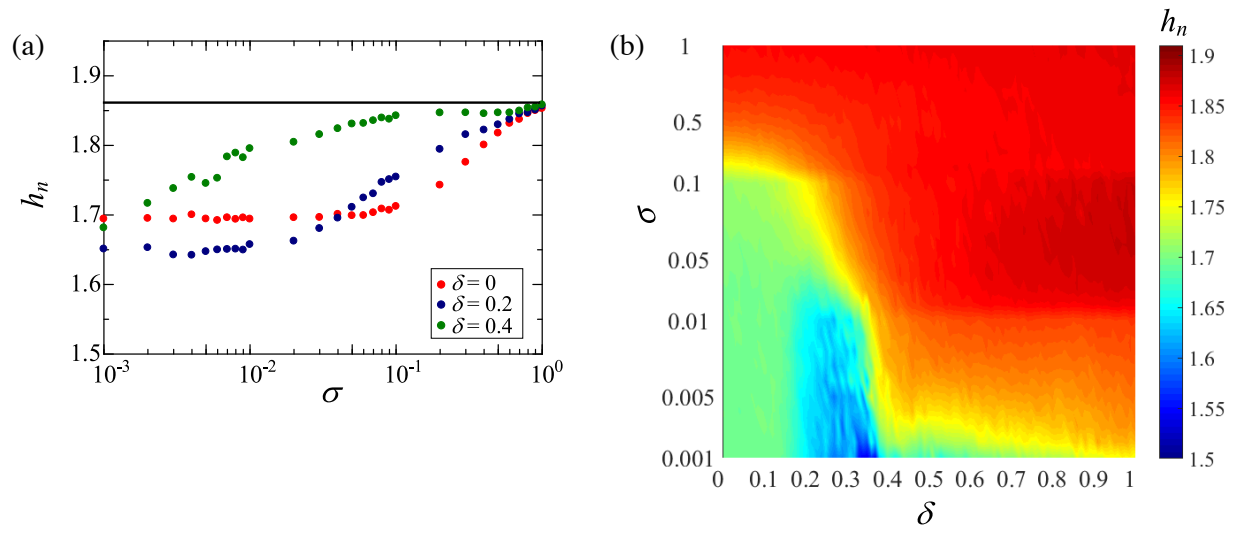

FIG. 7: (a) Network entropy h_n as function of σ for $\delta = 0$, 0.2, and 0.4. The solid line corresponds to the network entropy obtained from the EW equation. (b) Surface plot of h_n as function of δ and σ.

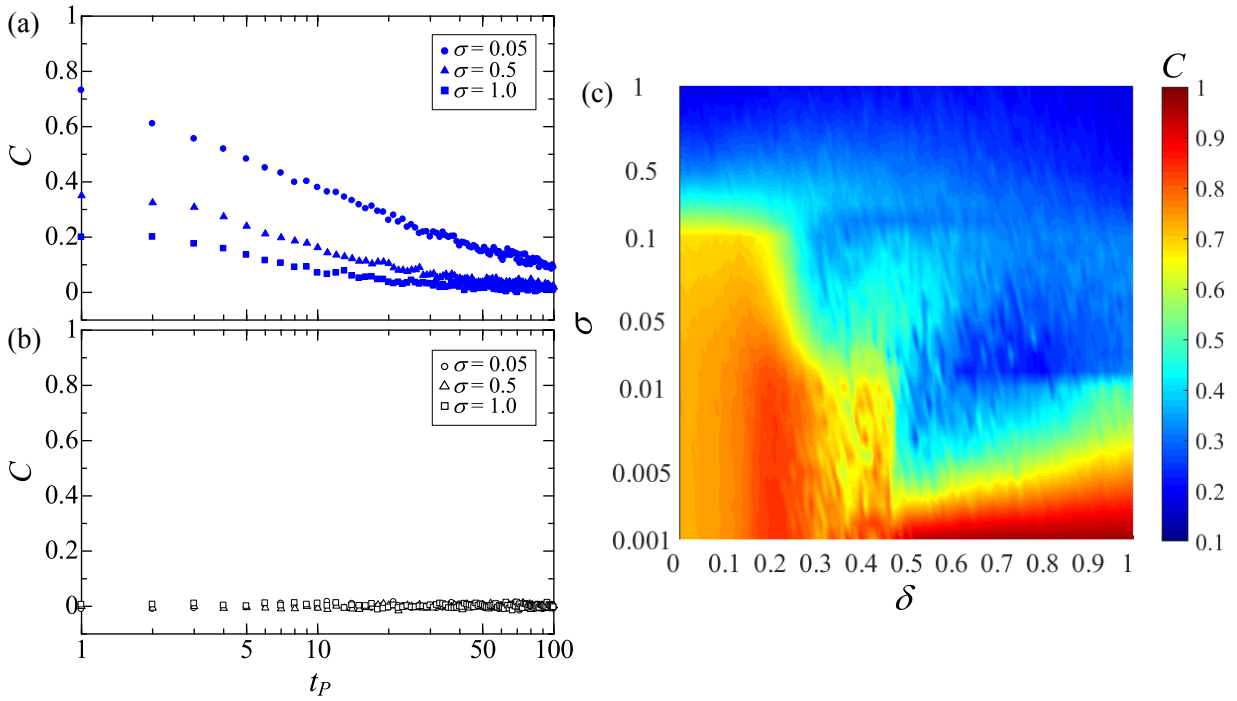

FIG. 8: Correlation coefficient C against the predicted time t_P for increment Δu_G with different values of σ for (a) noisy-gKS solution ($\delta = 0.2$) and (b) EW solution. Panel (c) shows the correlation coefficient $C(t_P = 1)$ as functions of σ and δ for Δu_G of the noisy gKS solution.

C. Nonlinear forecasting

Our previous study [52] using nonlinear forecasting demonstrated that for the deterministic chaos of the gKS equation, the dynamical behavior of the increment process $\Delta u_G (= (u_G(t_i + 1) - u_G(t_i))$ has strong correlation (> 0.8) between the predicted and original values at the prediction time $t_P = 1$, and the correlation coefficient C significantly decreases with t_P, showing the short-term predictability and long-term unpredictability dynamics. In the following, we apply the nonlinear forecasting methodology for both the increment process Δu_G of the noisy gKS and EW solutions to discuss its applicability under additive noise. Figure 8(a) depicts the variations of C in terms of t_P

for different σ. $C(t_P = 1)$ for u_G of the KS solution at $\sigma = 0.05$ is larger than 0.7, indicating that one-step-ahead prediction of the dynamical state is achieved with relatively high accuracy. C exponentially decays with t_P due to the long-term unpredictability characteristics of chaos. The important point to note here is that $C(t_P = 1)$ decreases with increasing σ owing to the effect of additive noise. In contrast, C for the EW solution is nearly zero regardless of t_P, as expected for purely stochastic process. This shows that the nonlinear forecasting for the increment process allows us to distinguish between a chaotic and a stochastic process. Variations of $C(t_P = 1)$ for Δu_G of the noisy gKS solution are shown in Fig. 8(b) as functions of σ and δ. We observe that for $\delta = 0$, C nearly remains unchanged up to $\sigma = 0.07$ with a value larger than the criteria of highly correlation (~ 0.7) between predicted and original values, indicating the persistence of the deterministic chaotic dynamics, until noise starts to dominate giving rise to a significant decrease in C. For $\delta = 0.2$, C is larger than the case for $\delta = 0$ for small additive noise but decays as the noise intensity is decreased, something that is more pronounced for $\delta = 0.4$. These results show a similar trend as in Figs. 4 and 7, albeit it is harder to clearly classify the three different regimes described above.

As a final remark, we note that the nonlinear forecasting methodology can also be used as a tool to investigate the existence of noise-induced low-dimensional chaos in other types of dynamical systems. An example of this is the noisy Lorenz equation for which Gao et al. [73] reported that the additive noise is able to induce a low-dimensional chaotic dynamics in an otherwise periodic oscillatory regime of the system. Following this study, we investigated here (not shown) the correlation coefficient of the $X(t)$ signal obtained from the the noisy Lorenz equation (see [73] for details of the equation) observing that it gives similar results to the correlation coefficient obtained from the increment process $\Delta X(t)$ suggesting indeed the possible existence of noise-induced low-dimensional chaos in that system, something that, on the other hand, we have not observed in the noisy gKS equation.

V. CONCLUSIONS

We have presented a systematic study of the dynamical state of the noisy gKS equation by making use of time-series analyses tools, namely permutation entropy and permutation spectrum based on symbolic dynamics, and network entropy based on complex networks. The temporal magnitude of the signal u_G defined by the second moment of the solution $u(x, t)$ is used as a global measure to accessing the dynamical properties of the system. We have also contrasted the results from the noisy gKS solution to the stochastic dynamics obtained by the EW equation in order to distinguish between stochastic and deterministic chaotic dynamics. The high-dimensional chaos observed for the noisy gKS equation for small values of δ retains the deterministic nature for sufficiently small additive noise. As the additive noise increases the gKS dynamics starts to coexist with stochastic effects, until it reaches a critical point σ_c at which the signal becomes purely stochastic: the randomness of the stochastically dominated dynamics in the noisy gKS solution is equivalent to that of the EW equation. We quantified this transition as function of the dispersion parameter δ, observing that σ_c decays exponentially with δ as it goes beyond the value $\delta_p = 0.15$ which we related to the transition from high- to low-dimensional chaos of the deterministic gKS equation. For larger values of δ, we found that a minimum level of noise is sufficient to make the signal fully stochastic independently of δ. These effects have been clearly demonstrated by using the concepts of permutation entropy, permutation spectrum and network entropy.

Acknowledgments

HG thanks the Department of Chemical Engineering of Imperial College for hospitality during a sabbatical visit. He was partially supported by a "Grant-in-Aid for Scientific Research (B) from the Ministry of Education, Culture, Sports, Science and Technology of Japan (MEXT)". MP and SK acknowledge the Department of Mechanical Engineering of Tokyo University of Science for travel support and hospitality during an academic visit. We acknowledge financial support from the European Research Council (ERC) Advanced Grant No. 247031.

[1] P. C. Hohenberg and J. B. Swift, Effects of additive noise at the onset of Rayleigh-Bénard convection, Phys. Rev. A **46**, 4773 (1992).

[2] O. Psenda, C. B. Briozzo, and M. O. Cáceres, External noise in periodically forced Rayleigh-Bénard convection, Phys. Rev. E **54**, 6944 (1996).

[3] N. Savva, G. A. Pavliotis, and S. Kalliadasis, Contact lines over random topographical substrates. Part 1. Statics, J. Fluid Mech. **672**, 358 (2011).

[4] N. Savva, G. A. Pavliotis, and S. Kalliadasis, Contact lines over random topographical substrates. Part 2. Dynamics, J. Fluid Mech. **672**, 384 (2011).

[5] E. A. Demekhin, E. N. Kalaidin, S. Kalliadasis, and S. Yu. Vlaskin, Three-dimensional localized coherent structures of surface turbulence. I. Scenarios of two-dimensional-three-dimensional transition, Phys. Fluids **19**, 114103 (2007).

[6] E. A. Demekhin, E. N. Kalaidin, S. Kalliadasis, and S. Yu. Vlaskin, Three-dimensional localized coherent structures of surface turbulence. II. Lambda solitons, Phys. Fluids **19**, 114104 (2007).

[7] W. Horsthemke, and R. Lefever, *Noise-Induced Transitions* (Springer, Berlin, 1984).

[8] F. Sagués, J.M. Sancho, and J. García-Ojalvo, Spatiotemporal order out of noise, Rev. Mod. Phys. **79**, 829 (2007).

[9] C. B. Muratov, E. Vanden-Eijnden, and E. Weinan, Noise can play an organizing role for the recurrent dynamics in excitable media, Proc. Nat. Acad. Sci. **104**, 702 (2007).

[10] E. Knobloch, Spatially localized structures in dissipative systems: open problems, Nonlinearity **21**, T45 (2008).

[11] S. M. Houghton, E. Knobloch, S. M. Tobias, and M. R. E. Proctor, Transient spatio-temporal chaos in the complex Ginzburg-Landau equation on long domains, Phys. Lett. A **374**, 2030 (2010).

[12] G. Shivashinsky and D. Michelson, On Irregular Wavy Flow of a Liquid Down a Vertical Plane, Prog. Theor. Phys. **63**, 2112 (1980).

[13] A. J. Babchin, A. L. Frenkel, B. G. Levich, and G. I. Sivashinsky, Nonlinear saturation of Rayleigh-Taylor instability in thin films, Phys. Fluids **26**, 3159 (1983).

[14] M. Munkel and F. Kaiser, An intermittency route to chaos via attractor merging in the Laser-Kuramoto-Sivashinsky equation, Physica D) **98**, 156 (1996).

[15] G. M. Homsy, Model equations for wavy viscous film flow, Lect. Appl. Math **15**, 191 (1974).

[16] R. Cuerno, H. A. Makse, S. Tomassone, S. T. Harrington, and H. E. Stanley, Stochastic model for surface erosion via ion sputtering: Dynamical evolution from ripple morphology to rough morphology, Phys. Rev. Lett. **75**, 4464 (1995).

[17] R. Cuerno and K. B. Lauritsen, Renormalization-group analysis of a noisy Kuramoto-Sivashinsky equation, Phys. Rev. E **52**, 4853 (1995).

[18] K. B. Lauritsen, R. Cuerno, and H. A. Makse, Noisy Kuramoto-Sivashinsky equation for an erosion model, Phys. Rev. E **54**, 3577 (1996).

[19] J. Buceta, J. Pastor, M. A. Rubio, and F. Javier de la Rubia, The stochastic stabilized Kuramoto-Sivashinsky equation: a model for compact electrodeposition growth, Phys. Lett. A **235**, 464 (1997).

[20] F. Frost and B. Rauschenbach, Nanostructuring of solid surfaces by ion-beam erosion, Appl. Phys. A **77**, 1 (2003).

[21] Y. Lou and P. D. Christofides, Feedback control of surface roughness in sputtering processes using the stochastic Kuramoto-Sivashinsky equation, Comput. Chem. Eng. **29**, 741 (2005).

[22] Y. Lou, G. Hu, and P. D. Christofides, Model predictive control of nonlinear stochastic partial differential equations with application to a sputtering process, AIChE J. **54**, 2065 (2008).

[23] M. Nicoli, E. Vivo, and R. Cuerno, Kardar-Parisi-Zhang asymptotics for the two-dimensional noisy Kuramoto-Sivashinsky equation, Phys. Rev. E **82**, 045202 (2010).

[24] M. Pradas, D. Tseluiko, S. Kalliadasis, D. T. Papageorgiou, and G. A. Pavliotis, Noise induced state transitions, intermittency, and universality in the noisy Kuramoto-Sivashinksy equation, Phys. Rev. Lett. **106**, 060602 (2011).

[25] M. Pradas, G. A. Pavliotis, S. Kalliadasis, D. T. Papageorgiou, and D. Tseluiko, Additive noise effects in active nonlinear spatially extended systems, Euro. J. Appl. Math. **23**, 563 (2012).

[26] M. Schmuck, M. Pradas, S. Kalliadasis, and G. A. Pavliotis, New stochastic mode reduction strategy for dissipative systems, Phys. Rev. Lett. **110**, 244101 (2013).

[27] M. Schmuck, M. Pradas, S. Kalliadasis, and G. A. Pavliotis, A new mode reduction strategy for the generalized KuramotoSivashinsky equation, IMA J. Appl. Math. **80**, 273 (2015).

[28] J. Topper and T. Kawahara, Approximate Equations for Long Nonlinear Waves on a Viscous Fluid, Phys. Soc. Jpn 44, 663-666 (1978).

[29] T. Kawahara, Formation of Saturated Solitons in a Nonlinear Dispersive System with Instability and Dissipation, Phys. Rev. Lett. 51, 381-383 (1983).

[30] P. M. J. Trevelyan and S. Kalliadasis, Dynamics of a reactive falling film at large Péclet numbers. I. Long-wave approximation, Phys. Fluids **16**, 3191 (2004).

[31] S. Kalliadasis, E. A. Demekhin, C. Ruyer-Quil, and M. G. Velarde, Thermocapillary instability and wave formation on a film falling down a uniformly heated plane, J. Fluid Mech **492**, 303 (2003).

[32] C. Ruyer-Quil and S. Kalliadasis, Wavy regimes of film flow down a fiber, Phys. Rev. E **85**, 046302 (2012).

[33] A. Akrivis, D. T. Papageorgiou, and Y.-S Smyrlis, Linearly implicit methods for a semilinear parabolic system arising in two-phase flows, IMA J. Num. Anal. **31**, 299 (2011).

[34] B. I. Cohen, J.A. Krommes, W. M. Tang, and M. N. Rosenbluth, Non-linear saturation of the dissipative trapped-ion mode by mode coupling, Nucl. Fusion **16**, 971 (1976).

[35] M. Sato and M. Uwaha, Step bunching as formation of soliton-like pulses in benney equation, Europhys. Lett. **32**, 639 (1995).

[36] C. Misbah and O. Pierre-Louis, Pulses and disorder in a continuum version of step-bunching dynamics, Phys. Rev. E **53**, R4318 (1996).

[37] M. Sato, M. Uwaha, and Y. Saito, Control of chaotic wandering of an isolated step by the drift of adatoms, Phys. Rev. Lett. **80**, 4233 (1998).

[38] D. Tseluiko and D. T. Papageorgiou, Dynamics of an electrostatically modified Kuramoto-Sivashinsky-Korteweg-de Vries equation arising in falling film flows, Phys. Rev. E **82**, 016322 (2010).

[39] E. Cerpa, A. Mercado, and A. F. Pazoto, Null controllability of the stabilized Kuramoto-Sivashinsky system with one distributed control, SIAM J. Control Optim. **53**, 1543 (2015).

[40] S. Gomes, M. Pradas, S. Kalliadasis, D. T. Papageorgiou, and G. A. Pavliotis, Controlling spatiotemporal chaos in active dissipative-dispersive nonlinear systems, Phys. Rev. E **92**, 022912 (2015).

[41] S. Kalliadasis, C. Ruyer-Quil, B. Scheid, and M. G. Velarde, Falling Liquid Films, Springer Series on Applied Mathematical Sciences, vol. 176 (Springer Berlin Heidelberg, 2012).

[42] N. J. Balmforth, Solitary Waves and homoclinic orbits, Annu. Rev. Fluid Mech. **27**, 335 (1995).

[43] H.-C. Chang, E. Demekhin, and E. Kalaidin, Interaction dynamics of solitary waves on a falling film, J. Fluid Mech. **294**, 123 (1995).

[44] S.-I. Ei, and T. Ohta, Equation of motion for interacting pulses, Phys. Rev. E **50**, 4672 (1994).

[45] C. Duprat, F. Giorgiutti-Dauphiné, D. Tseluiko, S. Saprykin, and S. Kalliadasis, Liquid film coating a fiber as a model system for the formation of bound states in active dispersive-dissipative nonlinear media, Phys. Rev. Lett. **103**, 234501 (2009).

[46] D. Tseluiko, S. Saprykin, and S. Kalliadasis, Interaction of solitary pulses in active dispersive-dissipative media, Proc. Est. Acad. Sci. **59**, 139 (2010).

[47] D. Tseluiko, S. Saprykin, C. Duprat, F. Giorgiutti-Dauphiné, and S. Kalliadasis, Pulse dynamics in low-Reynolds-number interfacial hydrodynamics: Experiments and theory, Physica D **239**, 2000 (2010).

[48] C. Duprat, D. Tseluiko, S. Saprykin, S. Kalliadasis, and F. Giorgiutti-Dauphiné, Wave interactions on a viscous film coating a vertical fibre: Formation of bound states, Chem. Eng. Process. **50**, 519 (2011).

[49] D. Tseluiko and S. Kalliadasis, Weak interaction of solitary pulses in active dispersivedissipative nonlinear media, IMA J. Appl. Math. **79**, 274 (2012).

[50] M. Pradas, D. Tseluiko, and S. Kalliadasis, Rigorous coherent-structure theory for falling liquid films: Viscous dispersion effects on bound-state formation and self-organization, Phys. Fluids **23**, 044104 (2011).

[51] M. Pradas, S. Kalliadaisis, and D. Tseluiko, Binary interactions of solitary pulses in falling liquid films, IMA J. Appl. Math. **77**, 408 (2012).

[52] H. Gotoda, M. Pradas, and S. Kalliadaisis, Nonlinear forecasting of the generalized Kuramoto-Sivashinsky equation, Int. J. Bifur. Chaos **25**, 1530015 (2015).

[53] G. Grün, K. Mecke, and M. Rauscher, Thin-Film Flow Influenced by Thermal Noise, J. Stat. Phys. **122**, 1261 (2006).

[54] M. A. Durán-Olivencia, R. S. Gvalani, S. Kalliadasis, G. A. Pavliotis, Instability, rupture and fluctuations in thin liquid films: Theory and computations, arXiv: 1707.08811 (2017).

[55] C. Bandt and B. Pompe, Permutation entropy: A natural complexity measure for time series, Phys. Rev. Lett. **88**, 174102 (2002).

[56] C. W. Kulp and L. Zunino, Discriminating chaotic and stochastic dynamics through the permutation spectrum test, Chaos **24**, 033116 (2014).

[57] B. Luque, L. Lacasa, F. Ballesteros, and J. Luque, Horizontal visibility graphs: Exact results for random time series, Phys. Rev. E **80**, 046103 (2009).

[58] K. R. Elder, J. D. Gunton, and N. Goldenfeld, Transition to spatiotemporal chaos in the damped Kuramoto-Sivashinsky equation, Phys. Rev. E **56** 1631 (1997).

[59] R. W. Wittenberg and P. Holmes, Scale and space localization in the KuramotoSivashinsky equation, Chaos **9**, 452 (1999).

[60] L. N. Trefethen, *Spectral methods in MATLAB*, SIAM (2000).

[61] A. K Kassam and L. N. Trefethen, Fourth-order time-stepping for stiff PDEs, SIAM J. Sci. Comput. **26**, 1214 (2005).

[62] J. Shen, Spectral Methods: Algorithms, Analysis and Applications, Springer Series in Computational Mathematics, vol. 41 (Springer Berlin Heidelberg, 2011).

[63] S. N. Gomes, M. Pradas, S. Kalliadasis, D. T. Papageorgiou, and G. A. Pavliotis, Controlling roughening processes in the stochastic Kuramoto-Sivashinsky equation, Physica D (2017), in press, DOI: 10.1016/j.physd.2017.02.011.

[64] P. Manneville, Macroscopic Modeling of Turbulent Flows, Lecture Notes in Physics. 230 (Springer Berlin Heidelberg, 1985).

[65] S. Domen, H. Gotoda, T. Kuriyama, Y. Okuno, and S. Tachibana, Detection and prevention of blowout in a lean premixed gas-turbine model combustor using the concept of dynamical system theory, Proc. Combust. Inst. **36**, 3245 (2016).

[66] C. Bian, C. Qin, Q. D. Y. Ma, and Q. Shen, Modified permutation-entropy analysis of heartbeat dynamics, Phys. Rev. E **85**, 021906 (2012).

[67] A. Aragoneses, L. Carpi, N. Tarasov, D. V. Churkin, M. C. Torrent, C. Masoller, and S. K. Turitsyn, Unveiling temporal correlations characteristic of a phase transition in the output intensity of a fiber laser, Phys. Rev. Lett. **116**, 033902 (2016).

[68] H. Gotoda, Y. Okuno, K. Hayashi, and S. Tachibana, Characterization of degeneration process in combustion instability based on dynamical systems theory, Phys. Rev. E **92**, 052906 (2015).

[69] H. Kinugawa, K. Ueda, and H. Gotoda, Chaos of radiative heat-loss-induced flame front instability, Chaos **26**, 033104 (2016).

[70] F. Takens, Dynamical Systems of Turbulence, Lecture Notes in Mathematics, vol. 898 (Springer Berlin Heidelberg, 1981).

[71] H. Gotoda, R. Takeuchi, Y. Okuno, and T. Miyano, Low-dimensional dynamical system for Rayleigh-Benard convection subjected to magnetic field, J. App. Phys. **113**, 124902 (2013).

[72] S. F. Edward and D. R. Wilkinson, The surface statistics of a granular aggregate, Proc. R. Soc. London A **381**, 17 (1982).

[73] J. B. Gao, W. W. Tung, and N. Rao, Noise-induced Hopf-bifurcation-type sequence and transition to chaos in the Lorenz equations, Phys. Rev. Lett. **89**, 254101 (2002).